Giant Conductivity Modulation of Aluminum Oxide Using Focused Ion Beam
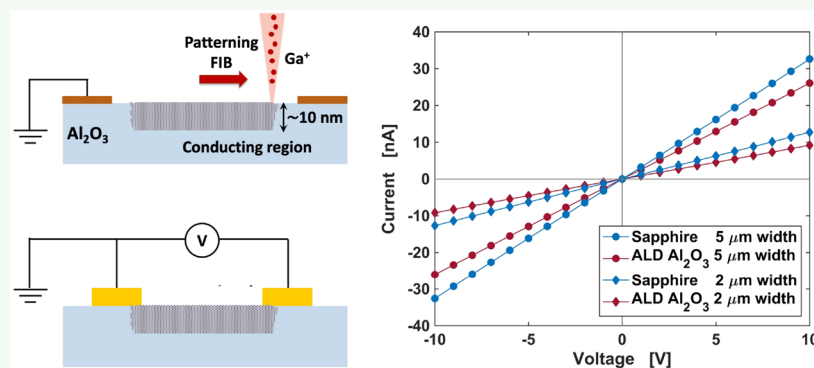
Simone Bianconi,[†] Min-Su Park,[†,‡] and Hooman Mohseni*,[†]

[†]Department of Electrical and Computer Engineering, Northwestern University, Evanston, Illinois 60208, United States
[‡]Nano Convergence Research Center Korea Electronics Technology Institute, 111 Ballyong-ro, Deokjin-gu, Jeonju 54853, South Korea

S *Supporting Information*

ABSTRACT: Precise control of the conductivity of semiconductors through doping has enabled the creation of advanced electronic devices; similarly, the ability to control the conductivity in oxides can enable novel advanced electronic and optoelectronic functionalities. While this was successfully shown for moderately insulating oxides, such as In_2O_3, a reliable method for increasing the conductivity of highly insulating, wide bandgap dielectrics, such as aluminum oxide (Al_2O_3), has not been reported yet. Al_2O_3 is a material of significant technological interest, permeating diverse fields of application, thanks to its exceptional mechanical strength and dielectric properties. Here we present a versatile method for precisely changing the conductivity of Al_2O_3. Our approach greatly exceeds the magnitude of the best previously reported change of conductivity in an oxide (In_2O_3). With an increase in conductivity of ∼14 orders of magnitude, our method presents ∼10 orders of magnitude higher change in conductivity than the best previously reported result. Our method can use focused ion beam to produce conductive zones with nanoscale resolution within the insulating Al_2O_3 matrix. We investigated the source of conductivity modulation and identified trap-assisted conduction in the ion damage-induced defects as the main charge transport mechanism. The temperature dependency of the conductivity and optical characterization of the patterned areas offer further insight into the nature of the conduction mechanism. We also show that the process is extremely reproducible and robust against moderate annealing temperatures and chemical environment. The record conductivity modulation combined with the nanoscale patterning precision allows the creation of conductive zones within a highly insulating, mechanically hard, chemically inert, and biocompatible matrix, which could find broad applications in electronics, optoelectronics, and medical implants.

KEYWORDS: *thin films, alumina, dielectrics, defect engineering, conducting oxides, focused ion beam*

INTRODUCTION

Aluminum oxide (Al_2O_3) is one of the most widely employed dielectric materials, thanks to its excellent insulating properties,[1] mechanical hardness and resistance,[2] and biocompatibility,[2,3] with applications ranging from device passivation[1,4−8] to MOSFET gate[9−13] as well as biomedical implants and antifouling passivation.[2,3,14,15] Electrical functionalization of Al_2O_3 via reliable and spatially accurate control of its conductivity could enable novel sensing technologies encompassing electrical contacts embedded in a mechanically hard, chemically inert, and electrically insulating dielectric matrix. In particular, as transparent conducting nanowires have attracted increasing attention for a wide range of applications in

optoelectronics,[16−18] there is great interest and technological potential for novel techniques for creating conducting nanowires in a widely employed transparent dielectric such as Al_2O_3. Examples of such technological applications include photon emission and detection,[7,19−22] low-energy interconnects,[23−25] energy conversion,[1,26,27] and implantable devices.[28−30]

We here present an effective method for the nonsubtractive nanopatterning of electrically conductive wires and other
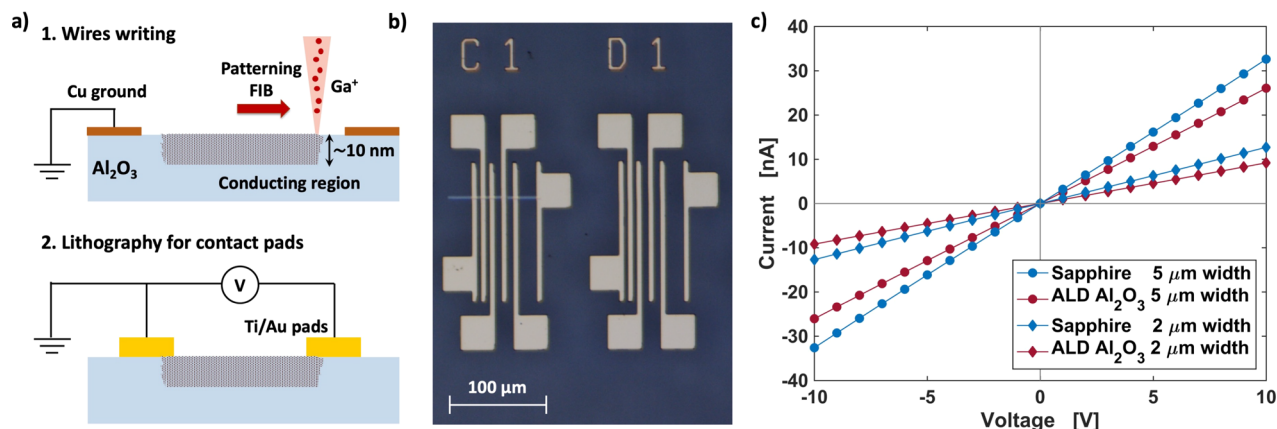
Figure 1. Method for patterning of conductive wires in Al_2O_3. (a) Schematic of the patterning and fabrication of the wires in Al_2O_3 matrix. (b) Microscope image of the fabricated devices including the contact pads and both implanted (left) and nonimplanted devices (right). (c) Ohmic current−voltage characteristics of patterned wires of varying widths implanted in bulk sapphire and ALD Al_2O_3.
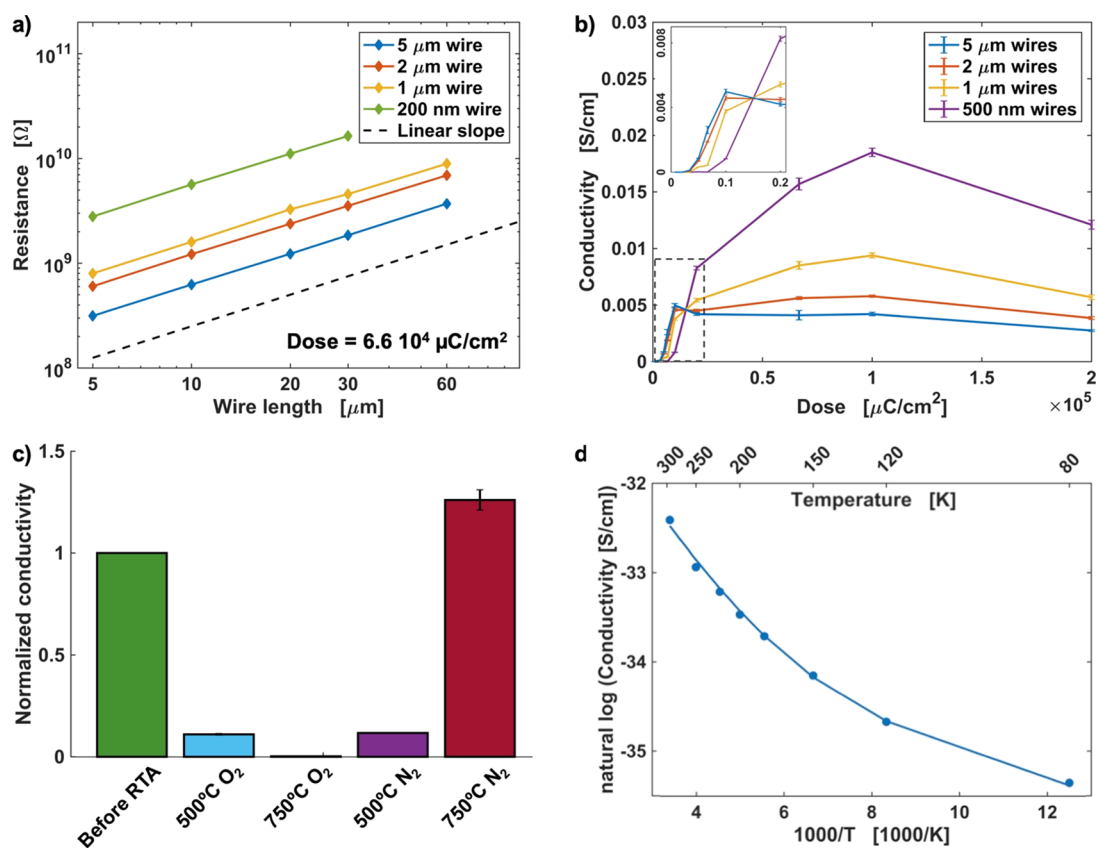

Figure 2. Electrical characterization of the patterned wires. (a) Resistance scales with the wire length and width. (b) Effect of ion dose on the wire conductivity. Error bars are calculated from a minimum of five devices per data point. (c) Effect of RTA treatment on the conductivity of patterned Al_2O_3 wires. Four different samples were treated with 15 s RTA in different environments and temperatures: the error bars are calculated from a minimum of three devices per data point. (d) Arrhenius plot of the conductivity of patterned wires. The solid lines represent the fit used to estimate the activation energies according to the model in eq 1.

features embedded in a dielectric Al_2O_3 substrate, using focused ion beam (FIB). Radiation-induced increase in conductivity of α-Al_2O_3 was first noticed as an anomalous detrimental effect on insulating properties upon irradiation from high-energy ions in nuclear instrumentation, designated as radiation-induced electrical degradation.[31,32] While large changes in conductivity have been reported upon exposure to high-energy, high-fluence radiation,[33,34] this effect has never been tuned or characterized for its employment in techno-

logical application. Concurrently, while patterning of nano-wires in transparent conductive In_2O_3 has been demonstrated by using FIB, the conductivity modulation was limited to 4 orders of magnitude.[35,36] Here, we show nanopatterning of conductive zones in highly insulating Al_2O_3, achieving a conductivity modulation of 14 orders of magnitude[37] (see the Supporting Information). To the best of our knowledge, this is the highest reported change in conductivity by using FIB.

FIB has proven to be an extremely effective tool for the nanopatterning of transparent conducting oxides (TCO) via lithographically controlled dopant implantation[35,36] as well as for structural modification and nonsubtractive patterning of dielectric substrates.[20,38] Despite being an inherently serial processing tool, FIB has shown very attractive potential in large-area milling and implantation, in particular when integrated with pattern generator lithography capabilities.[39−41] Furthermore, thanks to the higher beam deflection speed and lower settling time compared to electron beams, milling-based ion beam lithography (IBL) has demonstrated exposure times for large patterns that are comparable to those of EBL, and even faster patterning times can be achieved for ion implantation at lower dosage.[42]

RESULTS AND DISCUSSION

The process schematic of our method is presented in Figure 1: the fabrication process is fairly simple, highly tunable, and extremely versatile and can be applied to both bulk Al_2O_3 (i.e., sapphire) and thin film Al_2O_3 (e.g., ALD). To limit the effects of charging, inherent to FIB processing of insulating substrates, a metallic alignment pattern is deposited on the sample before implantation using lithographic techniques (Figure 1a). This metallic film serves a dual purpose: it is connected to ground during implantation, allowing to avoid excessive charging of the substrate, and facilitates the focusing and alignment of the ion beam, crucial for the subsequent processing steps. Alternatively, to further improve the spatial resolution of the patterned nanowires, an anticharging thin layer of Au can be deposited over the whole area of the sample before implantation, and subsequently removed, as proposed by Sosa et al.[35,36]

All the implanted wire-like structures exhibit ohmic behavior (Figure 1c). We argue that the mechanism behind this linear resistance is similar to the previously reported results from Ga- and Mg-implanted TCO layers.[33,34,36] Ohmic conduction in dielectrics has been observed at low field for a variety of oxides and is related to weak carrier injection from the contacts.[43,44] We tested our method for patterning wires in both bulk sapphire substrates and ALD-deposited Al_2O_3 films. As shown in Figure 1c, both matrices yield similar results in terms of the electrical conductivity; hence, the rest of this paper focuses on the results from bulk sapphire for brevity.

The electrical conductivity of the patterned nanowires is mainly determined by two factors: the geometrical size of the wires and the ion dose. As shown in Figure 2a, the electrical conductivity scales linearly with the wire length. Furthermore, the high fidelity of the measurements over the large number of fabricated devices proves the reproducibility and robustness of this method (see Table S2). The effect of implantation dose on the electrical characteristics of the wires is reported in Figure 2b: the conductivity of the nanowires varies by a few orders of magnitude within the range of doses explored. Notably, the conductivity reaches its maximum at a certain dose and then plateaus and falls off at higher doses. Moreover, such peaks occur at higher doses for thinner wires, possibly due to the raster scanning of the patterning ion beam, which allows for a better mitigation of the charging effect in larger-area patterns. Nanopatterning of smaller wires is characterized by a more localized charge, which could deflect the incident ion beam and result in a lower effective dose delivered to the substrate.[36]

DEVICE CHARACTERIZATION

Defect-Assisted Conduction. Several theoretical and experimental studies have advanced the hypothesis that damage-induced defects in electronic materials can create deep trap states in the bandgap, which intrinsically act as dopants, enabling electrical conduction in otherwise highly insulating materials.[36,45−50] These studies suggest that the electrical conductivity we observe in Al_2O_3 could be due to the formation of oxygen vacancies caused by the ion collision cascade.[33] To evaluate this hypothesis, we performed an annealing study as it was proved to be an effective tool for investigating the nature of the electrical conductivity in implanted wires in TCO.[36]

The results of rapid thermal annealing (RTA) treatment are presented in Figure 2c. Annealing at 750 °C in an oxidizing environment effectively erases the implanted wire, reducing the electrical conductivity to negligible levels, and thus presumably ruling out the implanted Ga ions as source of the conductivity in the wires. Conversely, annealing in a reducing environment (N_2) induces a higher conductivity in both the implanted wires and the nonimplanted Al_2O_3 matrix, as has been reported for similar mechanism in In_2O_3.[36] Indeed, reductive annealing is known to improve conductivity in TCOs by promoting oxygen vacancy formation, while oxidizing anneals results in the opposite effect.[36,51] These processes have been widely employed to modify and even cycle the conductivity in TCOs, confirming the disorder-induced nature of TCO doping, related to the formation of oxygen vacancies.[52−55] As shown in Figure 2c, RTA treatments performed at 500 °C result in a slight decrease in conductivity in both chemical environments, presumably due to incomplete activation of the defect annealing at such temperature. These results are consistent with published results for RTA treatment of similar implanted Ga nanowires in In_2O_3[36] and suggest that the electrical conductivity of the patterned wires is related to ion damage-induced chemical and structural modification of the Al_2O_3 matrix rather than to the implanted Ga ions.

Charge Transport. To further evaluate the nature of the charge transport mechanism, we performed temperature-dependent conductivity characterization of the implanted devices. Transport in a wide bandgap dielectric such as Al_2O_3 is typically governed by hopping conduction mechanisms of two types: direct trap-to-trap tunneling and phonon-assisted elastic and inelastic tunneling.[56−58] Presumably, both phenomena contribute to conduction in the implanted regions, as the momentum exchange via phonon scattering facilitates transport between trap states in parallel to direct tunneling. Both conduction mechanisms rely on an activation energy related to the thermal excitation of carriers at the trap sites, such that the temperature dependency of the conductivity, $\sigma = nq\mu$, can be modeled as[43,44]

$$\sigma = \alpha T^{-3/2} e^{-E_a/k_B T} \tag{1}$$

where α is a fitting parameter, k_B is Boltzmann's constant, and E_a is the activation energy in units of electronvolts. Figure 2d reveals a decrease in conductivity with the inverse of temperature, with two distinct characteristic energy scales within the range of temperatures investigated. Indeed, a good fit to the experimental data ($R^2 = 0.994$) is obtained by adding two exponential functions of the form of eq 1, which yield two estimated activation energies. Such dual behavior of temperature-dependent transport has been observed in similar
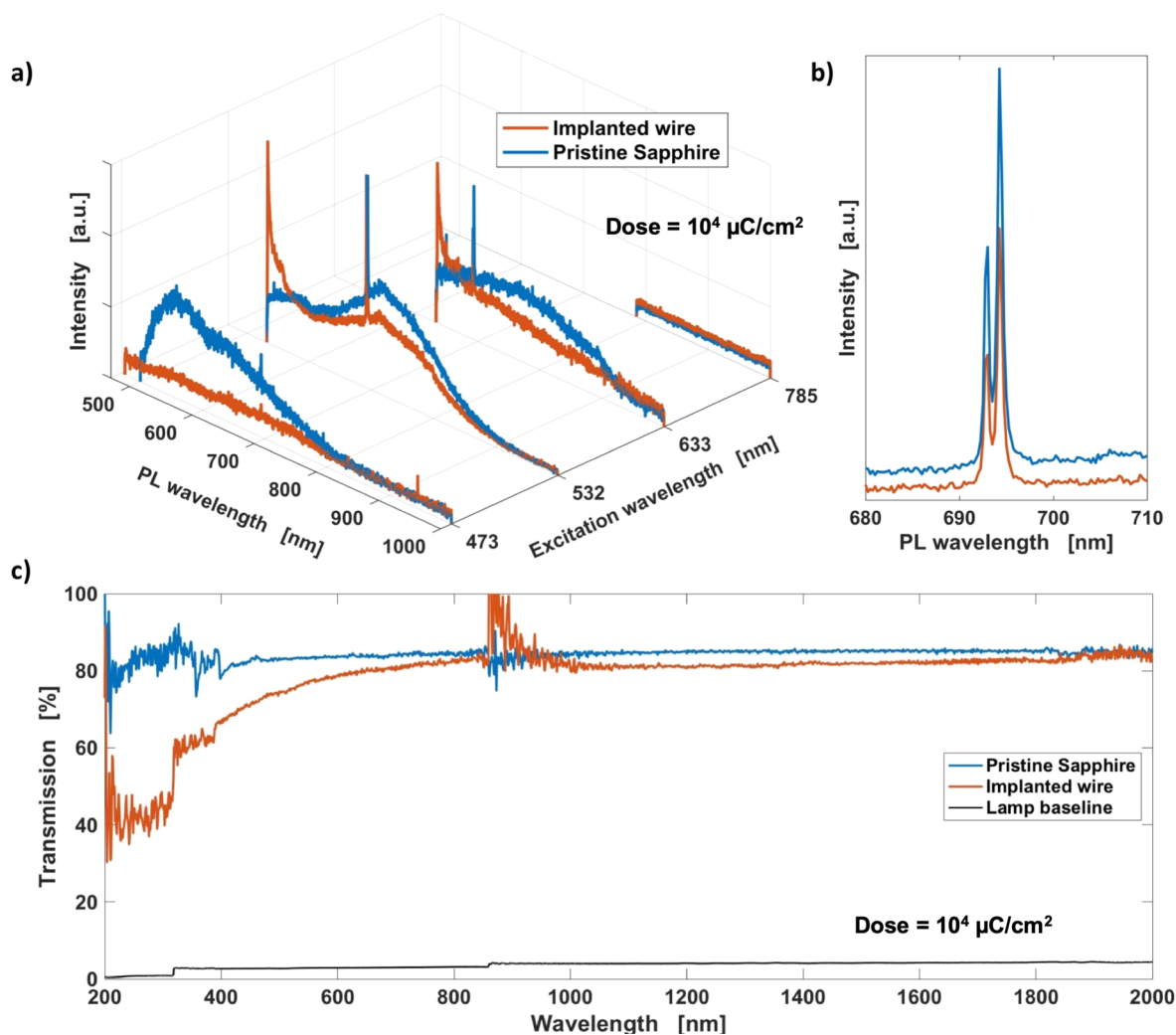
Figure 3. Optical and chemical characterization of the patterned wires. (a) PL maps of implanted wire (dose = 10^4 μC cm^{-2}) and pristine sapphire for different excitation wavelengths. (b) Particular of the photoluminescence spectrum for 532 nm excitation wavelength, showing the Cr^{3+} peaks for both implanted wire and pristine sapphire. (c) Optical transmission as a function of wavelength for implanted wire (dose = 10^4 μC cm^{-2}) and pristine sapphire.

disordered material systems.[59−61] We argue that in the high-temperature regime ($T > 200$ K) transport is dominated by phonon scattering, with a characteristic activation energy of 96 meV. At low temperatures, direct trap-to-trap tunneling constitutes the main conduction channel and is characterized by an activation energy scale of 50 meV.

Optical Characterization. Optical characterization has been utilized to evaluate the effects of the implantation on the sapphire substrate, specifically related to damage-induced interband defect states.[33] Figure 3 shows a significant change in the photoluminescence (PL) and transmission spectra of implanted samples compared to the pristine sapphire. These measurements support the argument for ion damage-induced formation of trap states within the oxide bandgap.[32−34,62] While the change in both PL and transmission due to implantation spans over a large range of wavelengths, interestingly, the characteristic Cr^{3+} impurity peak shown in Figure 3b is unaffected by the implantation process, hence suggesting a wider energy distribution of trap states in the bandgap as compared to atomic transition levels.[63,64] As a result, the implantation process results in a broad photo-luminescence band, which is in agreement with what has been

reported for ion-implanted Al_2O_3.[33] The luminescence of the implanted regions is higher than that of pristine sapphire at shorter wavelengths (see the curves for 532 and 633 nm excitation wavelengths in Figure 3a): this suggests the formation of optically active defect states deep in the oxide bandgap. Similarly, absorption at shorter wavelength is higher in the implanted regions, as shown in Figure 3c. Interestingly, the luminescence of the implanted Al_2O_3 is lower than that of pristine only for the shortest excitation wavelength of 473 nm: this may be due to additional recombination sites in the implanted regions, which activate at higher carrier energy.

■ CONCLUSION

We reported a novel method for nanopatterning of conductive zones in Al_2O_3 matrix using focused ion beam irradiation. The implanted wires exhibit ohmic conduction with an average conductivity of 10^{-2} S cm^{-1}. On the basis of a large number of measured devices, we showed that the presented nano-patterning process has excellent uniformity and nanoscale spatial resolution, while allowing for modulation of the electrical conductivity through control of the ion dose. The electrical, optical, and chemical characterizations provide

strong evidence that the conduction mechanism is due to the formation of trap states within the oxide bandgap. All processed devices showed stable performance during several months and after heating to 100 °C and immersion in liquid solvents. The present method shows great potential for application in sensing technologies that require electrical contacts embedded in a mechanically hard, chemically inert, and electrically insulating dielectric matrix. Examples of such applications include photon sensors, low-energy interconnects, and micro-/nanoimplantable medical devices.

■ EXPERIMENTAL SECTION

The majority of the devices presented were implanted in a 300 μm thick, double-side polished $\langle 0001 \rangle$ crystalline sapphire substrates. Some of the devices were implanted in an Al_2O_3 film deposited on both silicon and sapphire substrate using a Cambridge NanoTech Savannah S100 atomic layer deposition from trimethylaluminum and water vapor precursors at 150 °C. An 80 nm Cu layer with alignment mark pattern was deposited on the sample before implantation using photolithographic lift-off techniques. The metallic layer was connected to ground during implantation. A FEI Nova 600 NanoLab dual-beam microscope with a Sidewinder Ga^+ ion column and a 100 nm resolution piezomotor $X-Y$ stage was employed for the wire implantation at ion beam energies of 5 and 30 keV and currents of 100 pA, 3.2 and 6.3 nA, yielding estimated spot sizes ranging 20 to 60 nm. The instrument was combined with a RAITH Elphy 4.0 interface with integrated 16-bit DAC pattern generator, which enables large area patterning and write-field alignment, accounting for stitching and drift, and allows for precise dose control via beam blank and deflection. The Elphy interface allows for a multipass patterning technique, which helps contrast the strong charging in dielectrics. Nevertheless, we estimate the effective dose to be lower than the nominal value due to sputtering and localized charging deflecting the incident ions. The Ti/Au contacts were subsequently deposited with photolithographic lift-off techniques, and electrical testing was performed with a four-point probe station equipped with Agilent 4285A LCR meter. Photoluminescence spectra were acquired by using a HORIBA LabRAM HR Evolution confocal Raman, equipped with 473, 532, 633, and 785 nm lasers for excitation.

■ ASSOCIATED CONTENT

ⓢ Supporting Information

The Supporting Information is available free of charge on the ACS Publications website at DOI: 10.1021/acsaelm.9b00185.

Table S1: calculations of the magnitude of conductivity modulation in Al_2O_3 reported in this paper compared to that previously reported for In_2O_3;[35,36,45] Figure S1: additional proof for uniformity of the implanted conductive regions; Figure S2: additional graphic visualization of current−voltage characteristics after RTA treatments; Table S2: details of the fitting to the experimental data on the temperature dependency of conductivity reported in Figure 2d; Figure S3: Monte Carlo simulation of the full ion collision cascade, including straggle, range, sputtering, and displacement distribution; Figure S4: conductive AFM measurements of the conductivity profile of implanted conductive channels; Table S3: complete set of current−voltage measurements performed on all the fabricated devices (PDF)

■ AUTHOR INFORMATION

Corresponding Author

*E-mail hmohseni@northwestern.edu; Ph +1 (847) 491 7108.

ORCID ⓘ

Simone Bianconi: 0000-0002-3828-6513

Present Address

M.-S.P.: Nano Convergence Research Center, Korea Electronics Technology Institute 111 Ballyong-ro, Deokjin-gu, Jeonju 54853, South Korea.

Notes

The authors declare no competing financial interest.

■ ACKNOWLEDGMENTS

■ REFERENCES

(1) Belkin, A.; Bezryadin, A.; Hendren, L.; Hubler, A. Recovery of Alumina Nanocapacitors after High Voltage Breakdown. *Sci. Rep.* **2017**, *7* (1), 932.

(2) Thamaraiselvi, T. V.; Rajewari, S. Biological Evaluation of Bioceramic Materials - A Review. *Trends Biomater. Artif. Organs* **2004**, *81* (1), 9−17.

(3) Xifre-Perez, E.; Ferre-Borull, J.; Pallares, J.; Marsal, L. F. Mesoporous Alumina as a Biomaterial for Biomedical Applications. *Open Mater. Sci.* **2015**, *2* (1), 13−32.

(4) Gaboriau, D.; Boniface, M.; Valero, A.; Aldakov, D.; Brousse, T.; Gentile, P.; Sadki, S. Atomic Layer Deposition Alumina-Passivated Silicon Nanowires: Probing the Transition from Electrochemical Double-Layer Capacitor to Electrolytic Capacitor. *ACS Appl. Mater. Interfaces* **2017**, *9* (15), 13761−12769.

(5) Dingemans, G.; Engelhart, P.; Seguin, R.; Mandoc, M. M.; van de Sanden, M. C. M.; Kessels, W. M. M. Comparison Between Aluminum Oxide Surface Passivation Films Deposited with Thermal ALD, Plasma ALD and PECVD. 35th IEEE Photovoltaic Specialist Conference, Honolulu, HI, 2010.

(6) Miyajima, S.; Irikawa, J.; Yamada, A.; Konagai, M. High Quality Aluminum Oxide Passivation Layer for Crystalline Silicon Solar Cells Deposited by Parallel-Plate Plasma-Enhanced Chemical Vapor Deposition. *Appl. Phys. Express* **2010**, *3* (1), 012301.

(7) Park, M.-S.; Razaei, M.; Barnhart, K.; Tan, C. L.; Mohseni, H. Surface Passivation and Aging of InGaAs/InP Heterojunction Phototransistors. *J. Appl. Phys.* **2017**, *121* (23), 233105.

(8) Xin, Z.; Ling, Z. P.; Nandakumar, N.; Kaur, G.; Ke, C.; Liao, B.; Aberle, A. G.; Stangl, R. Surface Passivation Investigation on Ultra-Thin Atomic Layer Deposited Aluminum Oxide Layers for their Potential Application to Form Tunnel Layer Passivated Contacts. *Jpn. J. Appl. Phys.* **2017**, *56* (8S2), 08MB14.

(9) Hirama, K.; Takayanagi, H.; Yamauchi, S.; Jingu, Y.; Umezawa, H.; Kawarada, H. High-Performance p-Channel Diamond MOSFETs with Alumina Gate Insulator; IEEE International Electron Devices Meeting, Washington, DC, 2007.

(10) Gutiérrez, M.; Lloret, F.; Pham, T.; Cañas, J.; Reyes, D.; Eon, D.; Pernot, J.; Araújo, D. Control of the Alumina Microstructure to Reduce Gate Leaks in Diamond MOSFETs. *Nanomaterials* **2018**, *8* (8), 584.

(11) Zhang, L.; Guo, Y.; Hassan, V. V.; Tang, K.; Foad, M. A.; Woicik, J. C.; Pianetta, P.; Robertson, J.; McIntyre, P. C. Interface Engineering for Atomic Layer Deposited Alumina Gate Dielectric on SiGe Substrates. *ACS Appl. Mater. Interfaces* **2016**, *8* (29), 19110−19118.

(12) Si, M.; Su, C. J.; Jiang, C.; Conrad, N. J.; Zhou, H.; Maize, K. D.; Qiu, G.; Wu, C. T.; Shakouri, A.; Alam, M. A.; Ye, P. D. Steep-Slope Hysteresis-Free Negative Capacitance MoS2 Transistors. *Nat. Nanotechnol.* **2018**, *13* (1), 24−28.

(13) Peng, J.; Sun, Q.; Wang, S.; Wang, H.-Q.; Ma, W. Low-Temperature Solution-Processed Alumina as Gate Dielectric for Reducing the Operating-Voltage of Organic Field-Effect Transistors. *Appl. Phys. Lett.* **2013**, *103* (6), 061603.

(14) Dong, L.-x.; Yang, H.-w.; Liu, S.-t.; Wang, X.-m.; Xie, Y. F. Fabrication and Anti-Biofouling Properties of Alumina and Zeolite Nanoparticle Embedded Ultrafiltration Membranes. *Desalination* **2015**, *365*, 70−78.

(15) Feng, G.; Cheng, Y.; Wang, S.-Y.; Hsu, L. C.; Feliz, Y.; Borca-Tasciuc, D. A.; Worobo, R. W.; Moraru, C. I. Alumina Surfaces with Nanoscale Topography Reduce Attachment and Biofilm Formation by Escherichia Coli and Listeria spp. *Biofouling* **2014**, *30* (10), 1253−1268.

(16) Zhou, Z.; Lan, C.; Wei, R.; Ho, J. C. Transparent metal-oxide nanowires and their applications in harsh electronics. *J. Mater. Chem. C* **2019**, *7* (2), 202−217.

(17) Yip, S. P.; Shen, L.; Ho, J. Recent advances in III-Sb nanowires: from synthesis to applications. *Nanotechnology* **2019**, *30*, 202003.

(18) Tseng, J.-Y.; Lee, L.; Huang, Y.-C.; Chang, J.-H.; Su, T.-Y.; Shih, Y.-C.; Lin, H.-W.; Chueh, Y.-L. Pressure Welding of Silver Nanowires Networks at Room Temperature as Transparent Electrodes for Efficient Organic Light-Emitting Diodes. *Small* **2018**, *14* (38), 1800541.

(19) Mikhelashvili, V.; Cristea, D.; Meyler, B.; Yofis, S.; Shneider, Y.; Atiya, G.; Cohen-Hyams, T.; Kauffmann, Y.; Kaplan, W. D.; Eisenstein, G. A Highly Sensitive Broadband Planar Metal-Oxide-Semiconductor Photo Detector Fabricated on a Silicon-on-Insulator Substrate. *J. Appl. Phys.* **2014**, *116* (7), 074513.

(20) Wang, J.; Zhang, X.; Zhou, Y.; Li, K.; Wang, Z.; Peddibhotla, P.; Liu, F.; Bauerdick, S.; Rudzinski, A.; Liu, Z.; Gao, W. Scalable Fabrication of Single Silicon Vacancy Defect Arrays in Silicon Carbide Using Focused Ion Beam. *ACS Photonics* **2017**, *4* (5), 1054−1059.

(21) Jeske, J.; Lau, D. W.; Vidal, X.; McGuinness, L. P.; Reineck, P.; Johnson, B. C.; Doherty, M. W.; McCallum, J. C.; Onoda, S.; Jelezko, F.; Ohshima, T.; Volz, T.; Cole, J. H.; Gibson, B. C.; Greentree, A. D. Stimulated Emission from Nitrogen-Vacancy Centres in Diamond. *Nat. Commun.* **2017**, *8*, 14000.

(22) Rezaei, M.; Park, M.-S.; Tan, C. L.; Mohseni, H. Sensitivity Limit of Nanoscale Phototransistors. *IEEE Electron Device Lett.* **2017**, *38* (8), 1051−1054.

(23) Alimardani, N.; Conley, J. F. Enhancing Metal-Insulator-Insulator-Metal Tunnel Diodes via Defect Enhanced Direct Tunneling. *Appl. Phys. Lett.* **2014**, *105* (8), 082902.

(24) Miller, D. A. B. Physical Reasons for Optical Interconnections. *Int. J. Optoelectron.* **1997**, *11*, 155−168.

(25) Miller, D. Device Requirements for Optical Interconnects to Silicon Chips. *Proc. IEEE* **2009**, *97* (7), 1166−1185.

(26) Hu, S.; Shaner, M. R.; Beardslee, J. A.; Lichterman, M.; Brunschwig, B. S.; Lewis, N. S. Amorphous TiO$_2$ Coatings Stabilize Si, GaAs, and GaP Photoanodes for Efficient Water Oxidation. *Science* **2014**, *344*, 1005−1009.

(27) Liu, Y.; Stradins, P.; Deng, H.; Luo, J.; Wei, S.-H. Suppress Carrier Recombination by Introducing Defects: the Case of Si Solar Cell. *Appl. Phys. Lett.* **2016**, *108* (2), 022101.

(28) Kang, S.-K.; Hwang, S.-W.; Cheng, H.; Yu, S.; Kim, B. H.; Kim, J.-H.; Huang, Y.; Rogers, J. A. Dissolution Behaviors and Applications of Silicon Oxides and Nitrides in Transient Electronics. *Adv. Funct. Mater.* **2014**, *24* (28), 4427−4434.

(29) Fang, H.; et al. Ultrathin, Transferred Layers of Thermally Grown Silicon Dioxide as Biofluid Barriers for Biointegrated Flexible Electronic Systems. *Proc. Natl. Acad. Sci. U. S. A.* **2016**, *113* (42), 11682−11687.

(30) Diaz-Botia, C. A.; Luna, L. E.; Neely, R. M.; Chamanzar, M.; Carraro, C.; Carmena, J. M.; Sabes, P. N.; Maboudian, R.; Maharbiz, M. M. A Silicon Carbide Array for Electrocorticography and Peripheral Nerve Recording. *J. Neural Eng.* **2017**, *14* (5), 056006.

(31) Evans, B. D. A review of the optical properties of anion lattice vacancies, and electrical conduction in α-Al2O3: their relation to radiation-induced electrical degradation. *J. Nucl. Mater.* **1995**, *219*, 202−223.

(32) Townsend, P. D.; Chandler, P. J.; Zhang, L. *Optical Effects of Ion Implantation*; Cambridge University Press: 1994.

(33) Tardío, M.; González, R.; Ramírez, R.; Alves, E. Electrical conductivity in undoped α-Al2O3 crystals implanted with Mg ions. *Nucl. Instrum. Methods Phys. Res., Sect. B* **2008**, *266* (12−13), 2932−2935.

(34) Tardıo, M.; Ramırez, R.; González, R.; Chen, Y.; Kokta, M. High temperature semiconducting characteristics of magnesium-doped α-Al$_2$O$_3$ single crystals. *Appl. Phys. Lett.* **2001**, *79* (2), 206−208.

(35) Sosa, N. E.; Liu, J.; Chen, C.; Marks, T. J.; Hersam, M. C. Nanoscale Writing of Transparent Conducting Oxide Features with a Focused Ion Beam. *Adv. Mater.* **2009**, *21* (6), 721−725.

(36) Sosa, N. E.; Chen, C.; Liu, J.; Xie, S.; Marks, T. J.; Hersam, M. C. Nanoscale Structure, Composition and Charge Transport Analysis of Transparent Conducting Oxide Nanowires Written by Focused Ion Beam Implantation. *J. Am. Chem. Soc.* **2010**, *132* (21), 7347−7354.

(37) Dobrovinskaya, E. R.; Lytvynov, L. A.; Pishchik, V. *Sapphire*; 2009; p 55.

(38) Myers, B. D.; Stevens, B. L.; Rożkiewicz, D. I.; Barnett, S. A.; Dravid, V. P. Directed Assembly in Epitaxial Zinc Oxide Films on Focused Ion Beam Modified Sapphire Substrates. *J. Vac. Sci. Technol., B: Nanotechnol. Microelectron.: Mater., Process., Meas., Phenom.* **2012**, *30* (1), 010605.

(39) Palacios, E.; Ocola, L. E.; Joshi-Imre, A.; Bauerdick, S.; Berse, M.; Peto, L. Three-Dimensional Microfluidic Mixers Using Ion Beam Lithography and Micromachining. *J. Vac. Sci. Technol., B: Nanotechnol. Microelectron.: Mater., Process., Meas., Phenom.* **2010**, *28* (6), C6I1−C6I6.

(40) Ocola, L. E.; Palacios, E. Advances in Ion Beam Micromachining for Complex 3D Microfluidics. *J. Vac. Sci. Technol., B: Nanotechnol. Microelectron.: Mater., Process., Meas., Phenom.* **2013**, *31* (6), 06F401.

(41) Ocola, L. E.; Rue, C.; Maas, D. High-Resolution Direct-Write Patterning Using Focused Ion Beams. *MRS Bull.* **2014**, *39* (4), 336−342.

(42) Imre, A.; Ocola, L. E.; Rich, L.; Klingfus, J. Large Area Direct-Write Focused Ion-Beam Lithography with a Dual-Beam Microscope. *J. Vac. Sci. Technol., B: Nanotechnol. Microelectron.: Mater., Process., Meas., Phenom.* **2010**, *28* (2), 304−309.

(43) Chiu, F.-C. A Review on Conduction Mechanisms in Dielectric Films. *Adv. Mater. Sci. Eng.* **2014**, *2014*, 1−18.

(44) Wu, J.; Yin, B.; Wu, F.; Myung, Y.; Banerjee, P. Charge Transport in Single CuO Nanowires. *Appl. Phys. Lett.* **2014**, *105* (18), 183506.

(45) Sosa, N. E.; Chen, C.; Liu, J.; Marks, T. J.; Hersam, M. C. Large-Scale, Nonsubtractive Patterning of Transparent Conducting Oxides by Ion Bombardment. *Appl. Phys. Lett.* **2011**, *99* (2), 022110.

(46) Choi, M.; Lyons, J. L.; Janotti, A.; Van de Walle, C. G. Impact of Carbon and Nitrogen Impurities in High- Dielectrics on Metal-Oxide-Semiconductor Devices. *Appl. Phys. Lett.* **2013**, *102* (14), 142902.

(47) Choi, M.; Janotti, A.; Van de Walle, C. G. Native Point Defects and Dangling Bonds in -Al2O3. *J. Appl. Phys.* **2013**, *113* (4), 044501.

(48) Iberi, V.; Liang, L.; Ievlev, A. V.; Stanford, M. G.; Lin, M. W.; Li, X.; Mahjouri-Samani, M.; Jesse, S.; Sumpter, B. G.; Kalinin, S. V.; Joy, D. C.; Xiao, K.; Belianinov, A.; Ovchinnikova, O. S. Nanoforging Single Layer MoSe2 Through Defect Engineering with Focused Helium Ion Beams. *Sci. Rep.* **2016**, *6*, 30481.

(49) Madauß, L.; Ochedowski, O.; Lebius, H.; Ban-d'Etat, B.; Naylor, C. H.; Johnson, A. T. C.; Kotakoski, J.; Schleberger, M. Defect Engineering of Single- and Few-Layer MoS2 by Swift Heavy Ion Irradiation. *2D Mater.* **2017**, *4*, 015034.

(50) Nanda, G.; Goswami, S.; Watanabe, K.; Taniguchi, T.; Alkemade, P. F. Defect Control and n-Doping of Encapsulated Graphene by Helium-Ion-Beam Irradiation. *Nano Lett.* **2015**, *15* (6), 4006−4012.

(51) Cava, R.; Phillips, J. M.; Kwo, J.; Thomas, G.; Van Dover, R.; Carter, S.; Krajewski, J.; Peck, W., Jr.; Marshall, J.; Rapkine, D. GaInO3: A new transparent conducting oxide. *Appl. Phys. Lett.* **1994**, *64* (16), 2071−2072.

(52) Weijtens, C. Influence of the deposition and anneal temperature on the electrical properties of indium tin oxide. *J. Electrochem. Soc.* **1991**, *138* (11), 3432−3434.

(53) Ma, T. Y.; Shim, D. K. Effects of rapid thermal annealing on the morphology and electrical properties of ZnO/In films. *Thin Solid Films* **2002**, *410* (1−2), 8−13.

(54) Park, Y.-R.; Nam, E.-K.; Boo, J.-H.; Jung, D.-G.; Suh, S.-J.; Kim, Y.-S. Hydrogenated In-doped ZnO thin films for the new anode material of organic light emitting devices: synthesis and application test. *Bull. Korean Chem. Soc.* **2007**, *28* (12), 2396.

(55) Hwang, J.-H.; Edwards, D.; Kammler, D.; Mason, T. O. Point defects and electrical properties of Sn-doped In-based transparent conducting oxides. *Solid State Ionics* **2000**, *129* (1−4), 135−144.

(56) Jegert, G.; Popescu, D.; Lugli, P.; Häufel, M. J.; Weinreich, W.; Kersch, A. Role of Defect Relaxation for Trap-Assisted Tunneling in High- Thin Films: a First-Principles Kinetic Monte Carlo Study. *Phys. Rev. B: Condens. Matter Mater. Phys.* **2012**, *85* (4), 045303.

(57) Callewaert, F.; Hoang, A. M.; Razeghi, M. Generation-Recombination and Trap-Assisted Tunneling in Long Wavelength Infrared Minority Electron Unipolar Photodetectors Based on InAs/GaSb Superlattice. *Appl. Phys. Lett.* **2014**, *104* (5), 053508.

(58) Senthil Kumar, N.; Chandrasekaran, J.; Mariappan, R.; Sethuraman, M.; Chavali, M. V2O5 Nano-Rods Using Low Temperature Chemical Pyrophoric Reaction Technique: the Effect of Post Annealing Treatments on the Structural, Morphological, Optical and Electrical Properties. *Superlattices Microstruct.* **2014**, *65*, 353−364.

(59) Shewmon, P. *Diffusion in Solids*; Springer: 2016.

(60) Shirahama, S.; Zhang, S.; Aiba, M.; Inoue, H.; Hada, M.; Hayashi, Y.; Hata, K.; Tsuruoka, S.; Matsumoto, H. Temperature dependence of pressure-driven water permeation through membranes consisting of vertically-aligned double-walled carbon nanotube arrays. *Carbon* **2019**, *146*, 785−788.

(61) Srivastava, R. Investigation on temperature sensing of nanostructured zinc oxide synthesized via oxalate route. *J. Sens. Technol.* **2012**, *2* (1), 8.

(62) Wu, Z.; Türkler, A.; Brooks, R.; Hole, D. E.; Townsend, P. D.; Köster, S. F.; Kurt, K.; Gonzalo, J.; Suarez-Garcia, A. Luminescence Characterisation of Defects in Pld Alumina and Cu-Implanted Silica. *Nucl. Instrum. Methods Phys. Res., Sect. B* **2002**, *191*, 121−126.

(63) Kostyukov, A.; Baronskiy, M.; Rastorguev, A.; Snytnikov, V.; Snytnikov, V.; Zhuzhgov, A.; Ishchenko, A. Photoluminescence of Cr3+ in Nanostructured Al2O3 Synthesized by Evaporation Using a Continuous Wave CO$_2$ Laser. *RSC Adv.* **2016**, *6* (3), 2072−2078.

(64) Huang, C. C.; Al-Saab, F.; Wang, Y.; Ou, J. Y.; Walker, J. C.; Wang, S.; Gholipour, B.; Simpson, R. E.; Hewak, D. W. Scalable High-Mobility MoS2 Thin Films Fabricated by an Atmospheric Pressure Chemical Vapor Deposition Process at Ambient Temperature. *Nanoscale* **2014**, *6* (21), 12792−12797.